OPEN ACCESS

Biomedical Engineering ARTICLE

The Innovation Drug Discovery

# AI-driven discovery: A novel RANKL-targeting peptide for osteoporosis therapy

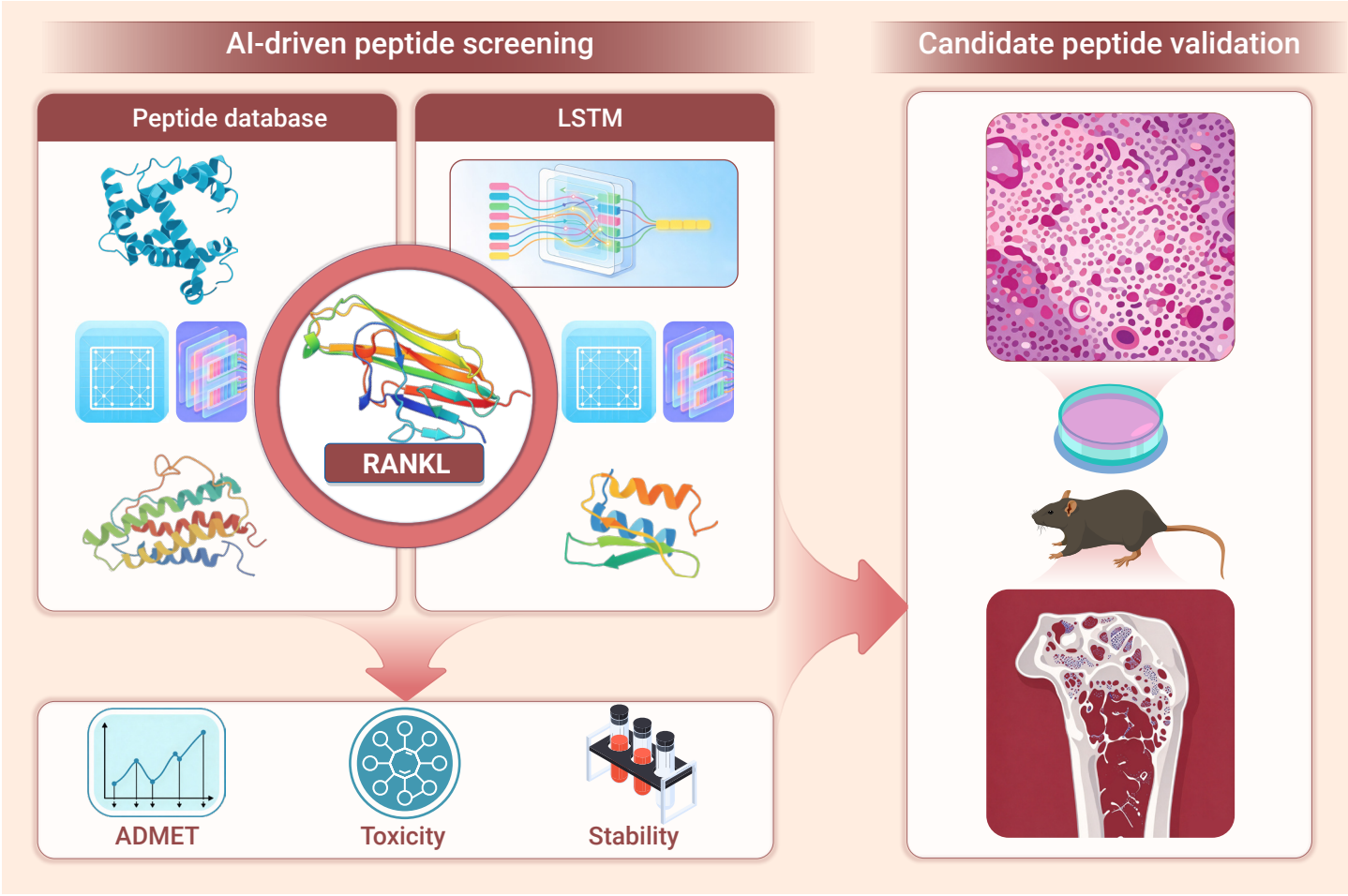
Zhiheng Chen,[1] Zehua Lu,[1] Yi Cui,[1] Ying Yu,[1] Chengxin Wang,[2] Chunyan Li,[2,*] and Xiaogang Wang[3,*]

*Correspondence: lichunyan@buaa.edu.cn(C.L.); xiaogangwang@smu.edu.cn(X.W.)

Received: May 26, 2026; Accepted: October 9, 2026; Published Online: October 14, 2026; https://doi.org/10.59717/j.xinn-drugdisc.2026.100041

© 2026 The Author(s). This is an open access article under the CC BY license (https://creativecommons.org/licenses/by/4.0/).

## GRAPHICAL ABSTRACT




## PUBLIC SUMMARY

- An AI-driven algorithm was employed to construct a high-affinity peptide library targeting RANKL.
- In vitro and in vivo studies confirmed that R-Peptide inhibits osteoclast differentiation and improves bone loss in OVX mice.
- Preliminary exploration was conducted into the potential mechanisms underlying R-Peptide's inhibition of osteoclast differentiation.

ARTICLE Biomedical Engineering

OPEN ACCESS



# AI-driven discovery: A novel RANKL-targeting peptide for osteoporosis therapy

**Zhiheng Chen,[1] Zehua Lu,[1] Yi Cui,[1] Ying Yu,[1] Chengxin Wang,[2] Chunyan Li,[2,*] and Xiaogang Wang[3,*]**

[1]School of Biological Science and Medical Engineering, Beihang University, Beijing 100083, China

[2]School of Engineering Medicine, Beihang University, Beijing 100083, China

[3]Guangdong Provincial Key Laboratory of Bone and Joint Degenerative Diseases, The Third Affiliated Hospital of Southern Medical University, Guangzhou 510630, China

*Correspondence: lichunyan@buaa.edu.cn(C.L.); xiaogangwang@smu.edu.cn(X.W.)

Received: May 26, 2026; Accepted: October 9, 2026; Published Online: October 14, 2026; https://doi.org/10.59717/j.xinn-drugdisc.2026.100041

© 2026 The Author(s). This is an open access article under the CC BY license (https://creativecommons.org/licenses/by/4.0/).

Citation: Chen Z., Lu Z., Cui Y., et al. (2026). AI-driven discovery: A novel RANKL-targeting peptide for osteoporosis therapy. *The Innovation Drug Discovery* **1**:100041.

The homeostasis between bone formation and resorption is essential for bone maintenance. Overactivation of bone resorption can lead to a decrease in bone density, an increase in bone fragility, and the development of osteoporosis. The Receptor Activator of Nuclear Factor κ B Ligand (RANKL) is a critical driver of bone resorption and a key therapeutic target for diseases like osteoporosis. Peptides, with their advantages of low immunogenicity and ease of synthesis, have emerged as promising drug candidates. Through a computational screening of approximately 100,000 peptide sequences using an AI-assisted strategy integrated with ADMET evaluation, we identified a novel class of RANKL-binding candidate peptides. Subsequent *in vitro* evaluation pinpointed R-Peptide as the lead candidate. *In vivo* validation further confirmed its anti-osteoclast effects in ovariectomized (OVX) mice and pro-osteogenic effects in wild-type (WT) mice. Mechanistically, R-Peptide significantly inhibited osteoclastogenesis by downregulating key marker genes (*Ctsk*, *Trap*, and *Nfatc1*) as well as critical components of the RANKL signaling pathway (RANKL and TRAF6). Taken together, this study identified a novel peptide that inhibits osteoclast differentiation and rescues bone loss in OVX mice, providing it as a promising therapeutic candidate for osteoporosis.

## INTRODUCTION

Bone is an essential tissue that constitutes the human skeletal system, providing mechanical support and maintaining vital physiological functions necessary for life.[1-2] Alterations in bone microstructure can lead to structural fragility and adversely affect an individual's quality of life.[2] The homeostasis between bone resorption and bone formation is essential for skeletal development and remodeling.[3] Age-related changes, genetic predisposition, and excessive bone resorption collectively contribute to the loss of bone mineral density and deterioration of microstructure, thereby increasing bone fragility and the risk of osteoporosis.[4-5]

The pathogenesis of osteoporosis involves a complex interplay of various cells and cytokines.[6] Notably, osteoclasts, derived from the monocyte/macrophage lineage in bone marrow, are the principal mediators of bone resorption and a key cellular culprit in pathological bone loss.[7-8] The nuclear factor kappa B ligand (RANKL), primarily produced by osteoblasts and some immune cells, binds to its receptor RANK.[9-10] The RANKL/RANK axis serves as a master regulator of bone resorption by activating downstream signaling pathways to promote osteoclastogenesis and resorptive activity, and the pathway overactivation will disrupt bone homeostasis, resulting in bone loss.[11-12]

Small molecule compounds,[13] nucleic acids,[14] and recombinant antibodies,[15] constitute the primary therapeutic modalities for various diseases. Peptides are gaining increasing recognition as their therapeutic value becomes more evident.[16] Teriparatide and abaloparatide are employed as therapeutics for osteoporosis,[17-18] whereas tirzepatide is approved for the treatment of metabolic disorders such as obesity.[19] As a distinct class of biologics, peptides occupy an intermediate niche between small molecules and large proteins. Typically comprising fewer than 50 amino acids, they offer a unique combination of favorable properties, including low immunogenicity, efficient tissue penetration, ease of synthesis, and cost-effective scalability, which underpin their broad and growing potential in drug development.[16,20-21]

Traditional drug screening methods are often time-consuming and costly.[22-23] However, the advent of computational strategies, such as virtual docking for library screening, offers a more efficient pathway to discover novel therapeutic targets.[24-26] In peptide drug discovery, libraries are frequently designed based on the known crystal structure of a protein that naturally binds the target receptor.[27] Alternatively, random peptide libraries, containing peptides of fixed or variable lengths, can be generated to uncover entirely new binding motifs. In both cases, computer-aided high-throughput virtual screening (HTVS) serves as a powerful and effective method for rapidly identifying high-affinity candidates from various biomolecular libraries.[28-29] This approach leverages algorithmic models, such as AutoDock,[30] to predict interaction affinities and thereby screen for potential therapeutic biomolecules.

Therapeutic strategies targeting RANKL have emerged as a promising approach for treating osteoporosis, driving the need for highly specific and stable inhibitors to aid in diagnosis and therapy.[31-32] To this end, we employed a structure-based drug design strategy. Utilizing the structure of the target RANKL protein, we constructed a peptide library and applied computational algorithms for virtual screening, leading to the discovery of potential high-affinity peptide molecules for osteoporosis treatment.

Given the pivotal role of RANKL in osteoclast maturation and differentiation, this study focuses on exploring peptide-based therapeutics targeting RANKL. By employing artificial intelligence algorithm tools, we identified a class of peptides with high affinity for RANKL. These candidates were subsequently screened based on ADMET prediction, followed by further evaluation of their stability and toxicity profiles. One peptide, designated as R-Peptide, emerged as the lead candidate. Its therapeutic effect, osteoclastogenesis inhibition via binding to RANKL, was validated both *in vitro* and *in vivo*. This study presents an innovative AI-driven strategy for peptide screening and offers a promising therapeutic approach for the treatment of osteoporosis.

## MATERIALS AND METHODS

### The library construction of active peptides and peptide screening

Peptide sequence information was collected from known peptide databases (Table S1), and the peptide library was established by sorting the number of amino acids in the peptide sequence and deleting the duplicates of peptide sequences.

### Virtual docking between candidate peptides and RANKL

First, download the pdb file of RANKL (PDB ID: 5BNQ) from the PDB database (https://www.rcsb.org), which contains three-dimensional structural information for proteins. The peptide sequences of the peptide library were docked and scored with the RANKL protein via AutoDock and PointNet tools. In short, the small-molecule-protein complex with PDB ID 5BNQ will be used to set up the docking box for the RANKL protein, ensuring that the docking box fully covers its docking molecules. First, the protein structure undergoes preprocessing, primarily dehydration and hydrogenation, followed by utilization of the software's grid box module. The x, y, and z dimensions in the AutoDock grid box parameters are set to 200 Å × 200 Å × 200 Å, with center coordinates at 55, 45, and 33, respectively, and a grid size of 0.375 Å. Subsequently, the peptide docking module is employed for docking. The structure of the peptide binding to the RANKL protein was demonstrated using PyMOL software (Figure 2A).

### Synthesis of candidate oligopeptides

Peptides with purity >99% were ordered from China Peptides Co., Ltd., each

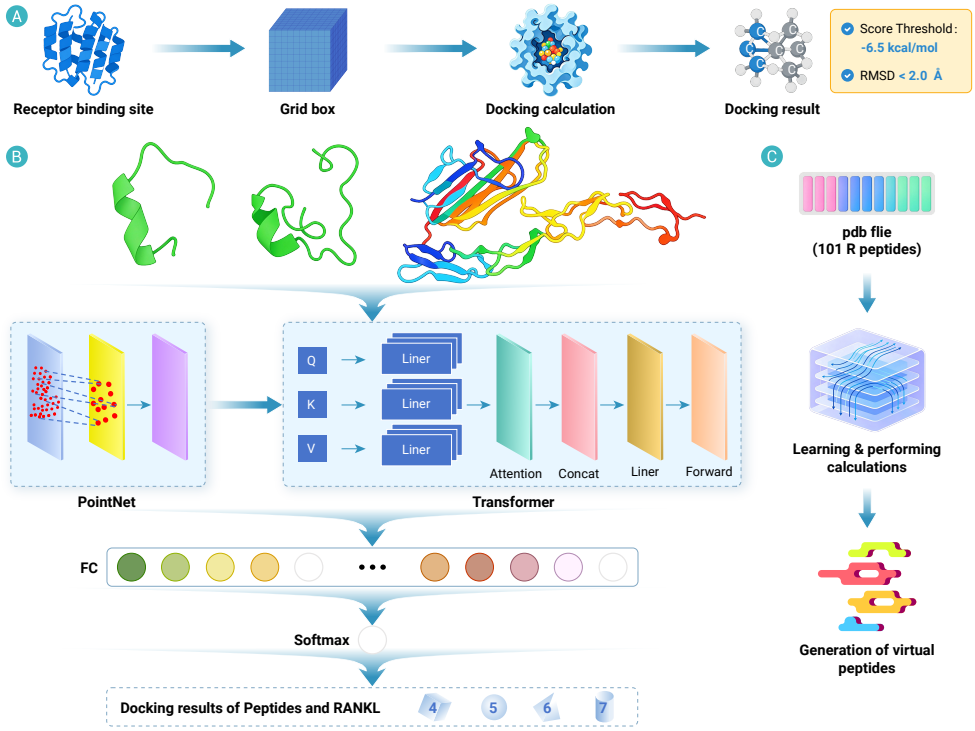



**Figure 1. Schematic diagram of the candidate peptide screening process** (A) Schematic diagram of the candidate peptide screening process using the AutoDock model. (B) Schematic diagram of the candidate peptide screening process using the PointNet model. First, the PointNet model converts the input of pdb files into three-dimensional point cloud data (in blue), which are further processed by the learning module Transformer. Transformer primarily identifies and captures amino acid binding information, and then records and learns the information. The Transformer consists of four components: the attention module (in green), to calculate amino acid binding weights and evaluate binding quality. Concat module (in pink) and Liner module (in brown): to convert 3D data into 1D. Forward module (in orange): to output the 1D results to subsequent modules. Subsequently, the learning module's output is converted into presentable data (e.g., scoring results) by the FC module. Finally, Softmax converts linear outputs into point clouds, enabling the visualization of docking results. (C) Schematic diagram of the generation of virtual candidate peptides using the LSTM model.

10 mg. HPLC and MALDI data were provided with lyophilized peptides. Peptides used in the *in vitro* assay were dissolved in saline to a final concentration of 0.1 mg/mL stock solutions and stored at −80°C for no more than two weeks. The molecular structure of the peptides was determined by ChemDraw software drawing (Figure S3, XN-R4578(MPKGSFNYAWVLDGLKAERWTGIDTGK)).

## ADMET prediction

To predict the drug toxicity of candidate peptides, we employed the ADMETlab 3.0 software (https://admetlab3.scbdd.com). First, the candidate peptide sequences were converted to SMILES format, then input into the website for evaluation.

## Stability testing

The stability of a 0.1 mg/mL peptide solution was determined at seven time points (0, 12, 24, 32, 48, 60, and 72 hours) using ultraviolet spectrophotometry. Results are shown in Figure S2.

## in vitro osteoclast differentiation

Mouse primary osteoclasts were differentiated from bone marrow-derived macrophages (BMMs) with the stimulation of M-CSF (Peprotech, #315-02) and RANKL (Peprotech, #315-11 C). Briefly, collect long bones from 8-week-old female C57BL/6J mice, then flush out bone marrow using a 1 mL syringe with serum-free α-MEM medium (Gibco, #12571-500). The bone marrow cells were suspended in growth medium (α-MEM + 10% FBS (Gibco, #10100-147)) and cultured for one day. Then, unattached cells were collected and adjusted to $3 \times 10^6$ cells/mL with α-MEM growth medium containing 50 ng/mL M-CSF and seeded in a cell culture dish for one day. Subsequently, they were exchanged to differentiation medium (50 ng/mL M-CSF + 100 ng/mL RANKL) and renewal medium every two days for a total of six days.

## TRAP staining

After dewaxing, the paraffin sections were immersed in PBS for 2 min. The TRAP staining was performed using a TRAP Staining Kit (Sigma, #387A) according to the manufacturer's instructions. Briefly, the slices were stained with the staining solution for 15 min at 37°C. Then, the slices were counterstained with hematoxylin solution (BBI, #E607318-0206) for 2 min and rinsed with ethyl alcohol. The sections were mounted with neutral resin after 10 min vitrification by dimethylbenzene. Pictures were taken using an inverted microscope (DS-Ri1, Nikon). Bone histomorphometric analyses for Oc.N/B.Pm and Oc.S/BS were performed using Bioquant Osteo software (v.7.20.10, Bioquant Nashville) according to the standard procedures published by the American Society for Bone Mineral Research.

## Plasmid transfection into cells

Lipofectamine™ 3000 Transfection Reagent was used for DNA transfection. Briefly, 2 μg of plasmid and 3.75 μL of P3000 reagent were added to the tube that included 125 μL of Opti-MEM medium, and vortexed for 10 s. Then, Lipofectamine 3000 reagent was added to the tube that included 125 μL of Opti-MEM medium and vortexed for 10 s, spun down, and incubated for 10 min at RT. Finally, the transfection complex was added to the 6-well plate and incubated for 6 hours. Then, the medium was changed, and the cells were cultured for 24 hours before sampling. The R-Peptide plasmid (containing His-tag) was synthesized by IBSBio (Shanghai, China).

## Quantitative real-time PCR assay (qPCR)

The TRIzol Reagent (Vazyme, #R411-02) was used for total RNA isolation from cultured cells and bone tissues. The PrimeScript RT Reagent Kit with gDNA Eraser Kit (Vazyme, #R333-01) was used for cDNA synthesis. The qPCR assays were conducted on a CFX96 Touch Real-Time PCR Detection System (Bio-Rad) using a TB Green Premix Ex Taq II Kit (Vazyme, #Q711-02) according to the manufacturer's instructions. Data were analyzed by CFX Manager 3.0 software (Bio-Rad). The gene expression levels were normalized with an internal housekeeping gene, GAPDH. Gene-specific primer sequences are listed in Table S4.

## Biotin pull-down assay

The pull-down assay was conducted using a biotin-labeled protein pull-down kit (Agarose Resin) (Beyotime, P0654S, Shanghai, China) to detect the binding between R-Peptide and RANKL. In brief, biotin-labeled R-Peptide was incubated with Streptavidin Agarose Resin, and unbound components were washed away. Then, the target protein (RANKL (Gibco, 310-01-10UG, USA)) was added to incubate with the above complex overnight at 4°C. The proteins eluted and recovered from the RANKL-R-Peptide-Streptavidin Agarose Resin complex were identified by Coomassie Brilliant Blue staining. analysis.

## Co-IP assay

In the Co-IP assay, the Anti-His (HHHHHH)-tag FAST IP Kit (Elabscience, EA-IP-K004, Wuhan, China) was used to detect the interaction between R-peptide and proteins in cells. In brief, plasmids encoding His-tagged R-Peptide (His-RP) were transfected into MLOY-4 cells, and qPCR was used to confirm that R-peptide was overexpressed. The protein lysates containing His-RP were incubated with Anti-His affinity gel (experimental group) or Mouse IgG affinity gel (negative control group) at 4°C overnight. The proteins

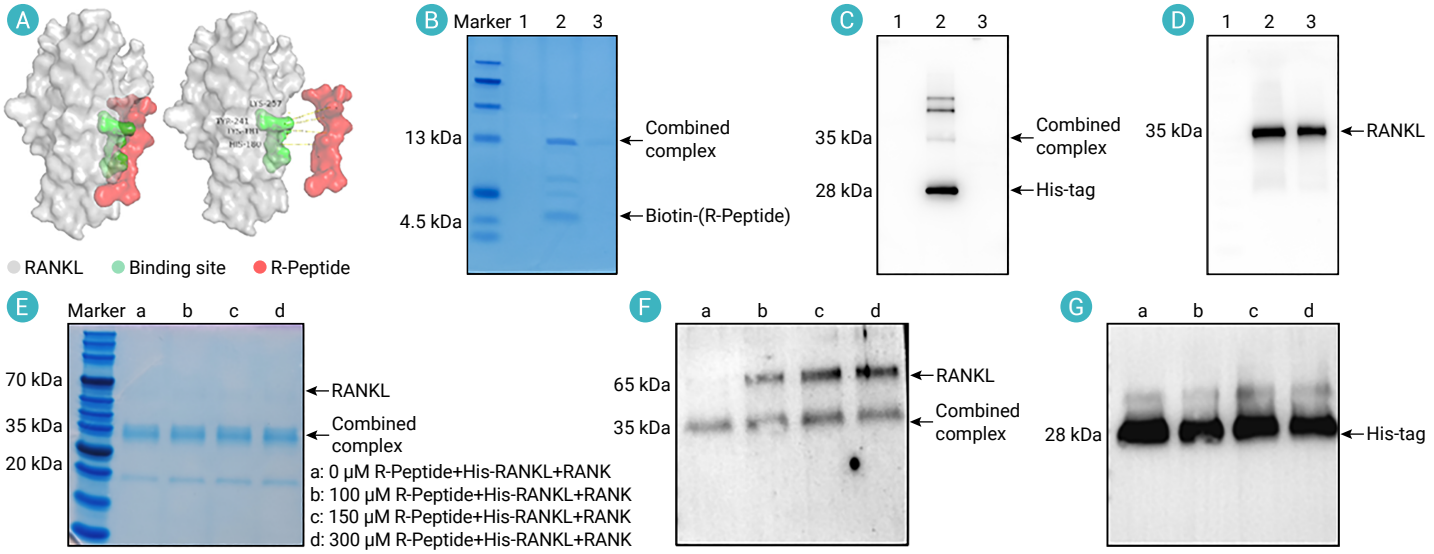



**Figure 2. The interaction between R-Peptide and RANKL** (A) Schematic diagram of the docking of the candidate peptide to the RANKL protein generated by PyMOL. (B) Validation of the R-Peptide-RANKL interaction by pull-down assay. Lane 1: PBS. Lane 2: biotinylated R-Peptide + RANKL. Lane 3: non-biotinylated R-Peptide + RANKL. Arrows indicate the RANKL-R-Peptide complex (Combined complex) and the free Biotin-R-Peptide (Biotin-R-Peptide). (C) Co-IP assay confirms intracellular interaction between the R-Peptide and RANKL. Lane 1: IgG negative control. Lane 2: experimental lane transfected with His-tagged RP plasmid. Lane 3: input lysate. The arrow indicates the His-RP band. (D) Western-blot analysis of RANKL following Co-IP. The arrow indicates the specific band for RANKL. (E) Validation of the R-Peptide's effect on the RANK-RANKL interaction by His pull-down assay. Lane a: His-RANKL + RANK. Lane b: 100 μM R-Peptide + RANKL + RANK. Lane c: 150 μM R-Peptide + RANKL + RANK. Lane d: 300 μM R-Peptide + RANKL + RANK. Arrows indicate the RANKL-R-Peptide complex (Combined complex) and RANK. (F) and (G) Western blot analysis of His pull-down samples. (F) Immunoblotting with an anti-RANK antibody; arrows indicate RANK and the combined complex, respectively. (G) Immunoblotting with an anti-His tag antibody; arrows indicate the His-tagged RNAKL.

eluted from these complexes were then detected by Western-blot.

## Western-blot assay

Cells were rinsed once with ice-cold PBS, then scraped from plates using SDS lysis buffer (Beyotime, #P0013G) containing protease inhibitors (Beyotime, #P1005), and lysed at 100°C for 10 min. Then, centrifugation at 12,000 × g for 10 min at 4°C to collect the supernatant, and measure the protein concentrations by the BCA Protein Assay Kit (Beyotime, #P0012S). Proteins were separated by SDS-PAGE and transferred to PVDF membranes (Millipore, IPVH0010), after blocking with 5% w/v nonfat milk at RT for 1 hour, the membranes were incubated with specific primary antibodies overnight at 4°C. Subsequently, the membranes were incubated with HRP-conjugated secondary antibodies at RT for 1 hour. Blots were visualized by a chemiluminescence reagent (Millipore, #WBLUR0500). The band density was quantified using Quantity One Software (v4.62, Bio-Rad). The primary antibodies included anti-His-tag (Elabscience, #E-AB-40506, 1:5000) anti-RANK (Biorbyt, #orb771527, 1:1000), anti-RANKL (Proteintech, #66610-1-AP, 1:3000), anti-NF-κB (Abcam, #ab16502, 1:1000), anti-TRAF6 (Affinity, #AF5376, 1:1000), anti-GAPDH (Sigma, #AMAB91153, 1:1000), Anti-mouse IgG, HRP-linked Antibody (Proteintech, #SA00001-1, 1:1000) and Anti-rabbit IgG, HRP-linked Antibody (Proteintech, #SA00001-2, 1:1000).

## His pull-down assay

Ten micrograms of purified His-RANKL (MCE, #HY-P78376) were dissolved in 100 μL PBS buffer containing 5% trehalose, loaded onto resin (Beyotime, P2247S, Shanghai, China) at room temperature for 45 min. Subsequently, R-Peptide compounds were added to each tube containing 10 μg of resolved RANKL at final concentrations of 100 μM, 150 μM, and 300 μM, and incubated for an additional 30 min. Thereafter, 2 μg of RANK (MCE, #HY-P71912) was added to each tube; after gentle mixing, incubation for an additional 20 min, followed by overnight incubation at 4°C. PBS buffer containing 5% trehalose served as the control group, with the procedure being identical. Resin was centrifuged, washed three times with 1 mL PBS, and resuspended in 2×SDS gel loading buffer. Samples were denatured at 100°C for 5 min. Denatured samples were analyzed by SDS-PAGE electrophoresis. Gels were immersed in Coomassie Brilliant Blue staining solution and eluted overnight on an oscillator. Concurrent Western blot analysis was performed using anti-RANK and anti-His antibodies, respectively.

## Animals

C57BL/6J mice were purchased from the Laboratory Animal Center of Capital Medical University and housed in a barrier environment in the School of Medical Science and Engineering, Beihang University. They are housed in a controlled environment with a temperature range of 20-26°C and humidity levels between 40% and 70% under a 12-hour light/dark cycle. These mice were fed irradiated chow (F003 for maintenance feeding, SPF (Beijing) Biotechnology Co., Ltd., Beijing, China) and had free access to drinking water.

## Establishment of an OVX mouse model

Bilateral ovarian removal surgery was performed to construct an OVX mouse model. Since females have a higher probability of developing osteoporosis, in this study, only female mice were selected for this experiment. Briefly, 12-week-old female mice are anesthetized with isoflurane and aseptically operated on both sides of their backs. After both ovaries are removed, the openings are sutured. After 12 weeks of surgery, the candidate peptide was injected subcutaneously at 1 mg/kg per injection each time, five times a week, for eight weeks.

## Micro-CT analysis

The right femur collected by micro-CT (μCT 50, Scanco Medical, Switzerland) was scanned for mice. The scanning resolution of one layer was set to 14.8 μm. Representative reconstructed images of the femur were taken separately to refer to the morphology of the distal growth plate. The threshold for Micro-CT was set from 212 to 1,000. Micro-CT image data were reconstructed and analyzed using Mimics software (v.13.0, Materialize NV).

## Enzyme-linked immunosorbent assay (ELISA)

The concentrations of TRAP-5b and S-CTX were detected by detecting serum samples from mice using an ELISA development kit. It is determined according to the manufacturer's instructions (#MM-45217M1, #MM-44696M1, Jiangsu Meimian Industrial Co., Ltd, China). The results of the experiment were repeated in triplicate.

## Immunofluorescence (IF) Staining

In brief, paraffin sections containing spleen tissue undergo dewaxing and dehydration, followed by overnight incubation with anti-CD4 and anti-CD8 antibodies (Servicebio, #GB15064, #GB15068) at 4°C. After three washes

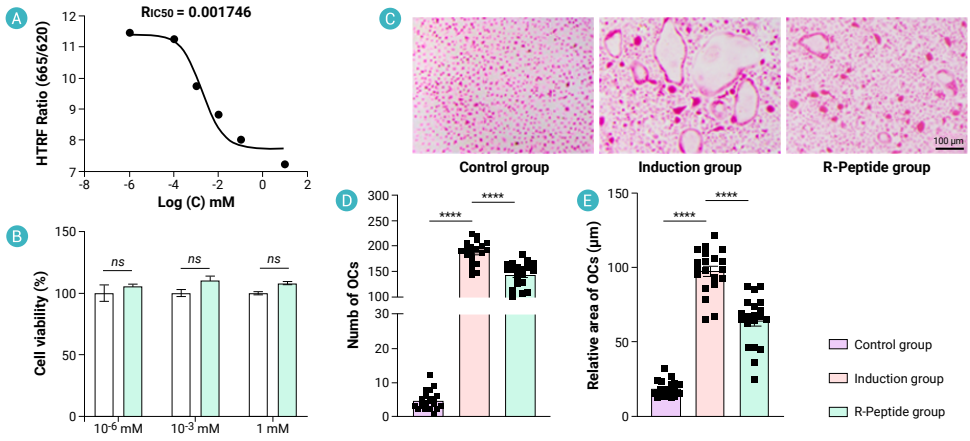



**Figure 3. R-Peptide inhibits osteoclast differentiation** (A) $IC_{50}$ of the R-Peptide, n = 3. (B) Cytotoxicity, n = 3. (C) The representative TRAP staining results. Scale bar, 100 μm. (D) Quantification of osteoclast number, n = 20. (E) Quantification of osteoclast volume, n = 20. $^{ns}$ $p > 0.05$, **** $p < 0.0001$.

with 1×PBS, incubate the samples with fluorescence-conjugated secondary antibodies for 2 hours at room temperature. Following three additional washes with 1×PBS, mount the slides with DAPI-containing anti-fluorescence quenching mounting medium. Observe and photograph under a fluorescence microscope. The CD4+/CD8+ cell ratios were calculated using ImageJ software (version: Fiji). Paraffin sections of bone, spleen, liver, and kidney were subjected to the same staining procedure using antibodies against TNF-α (Servicebio, #GB12188) and IL-6 antibodies (Servicebio, #GB11117). Stained sections were then visualized and photographed under a fluorescence microscope.

### H&E staining

Mouse femurs were decalcified in 10% EDTA solution for 28 days, and the solution was updated every 7 days. The femur and other organs were dehydrated by an automatic dehydrator (Microm STP120, Thermo). After embedding in paraffin, the tissue was sliced at 4 μm thickness by a rotary microtome (Microm HM325, Thermo). The slices are then deparaffinized in xylene and fractionated ethanol and then immersed in water for two minutes. Sections were stained with hematoxylin solution (BBI, #E607318-0206) for 1 min, differentiated in PBS for 5 min, and then stained with eosin solution (BBI, #E607318-0206) for 10 s and rinsed with water. Vitrified with dimethylbenzene for 10 min and then mounted with neutral resin. Photographs were taken using an inverted microscope (DS-Ri1, Nikon).

### Protein-Protein interaction prediction

Use the STRING online tool (https://cn.string-db.org) to predict potential interactions between RANKL and its associated proteins.

### Statistical analysis

All data are presented as the mean ± SEM for n ≥ 3. Significant differences between two groups were determined by an unpaired Student's t-test (two-tailed). Significant differences between multiple groups were determined by one-way analysis of variance (ANOVA) followed by Tukey's tests. A p-value of less than 0.05 was considered statistically significant. GraphPad Prism version 8.0 was used for all statistical analyses.

## RESULTS

### Identification of high-affinity candidate peptides

We first collected the information from the currently published peptide database (Table S1). A total of 107,593 peptide sequences, typically ranging from 2 to 50 amino acids in length, were remained after sorting and removal of redundant sequences. Since peptides with too few amino acids compromise stability, while those with too many amino acids could increase synthesis complexity, we selected sequences containing 10 to 30 amino acids from the 107,593 peptide sequences for further analysis. Consequently, a library of 2218 natural candidate peptides was established, and the amino acid sequences of these natural candidate peptides were converted to PDB files via Swiss-model tools (https://swissmodel.expasy.org/). The three-dimensional structural information of RANKL was downloaded from the Protein Data Bank (PDB). First, we employed a mature molecular docking model, AutoDock, to perform docking analysis on the aforementioned 2218 natural candidate peptides (Figure 1A). Given that the docking model PointNet utilizes its Transformer module to learn and compute peptide features, we conducted local training of this model based on documented binding data of RANKL and small molecules. Subsequently, a fully connected (FC) layer transformed the learned features into a one-dimensional scoring array. Finally, a Softmax layer was applied to generate the docking predictions for all 2218 natural candidate peptides (Figure 1B). Here, we got the docking scores from two independent computational tools, AutoDock and PointNet. Using defined thresholds, AutoDock identified 193 peptides with docking scores below -6.5 kcal/mol and PointNet screened out 185 peptides with docking scores greater than 6.5. Notably, 35 peptides were shared by both AutoDock and PointNet. To broaden the candidate pool, we integrated the top 36 peptides from the AutoDock analysis, the top 30 peptides from the PointNet analysis, and the 35 common peptides. This yielded a final set of 101 natural peptides (designated as "R peptides"; Figure S1).

Based on the docking characteristics of these 101 R peptides, we employed a sequence-based generative model, Long Short-Term Memory (LSTM) network, to construct a virtual peptide library (Figure 1C). First, the pdb files from these 101 R peptide sequences and the RANKL were input into this model. By learning the data features of these peptide sequences (primarily binding properties) and undergoing fine-tuning (learning commonalities between sequences), the model ultimately generated a second library of 3,692 virtual peptide sequences (designated as XN-R peptides), which were subsequently subjected to docking analysis using both AutoDock and PointNet. The docking results of the top 20 natural and virtual peptides are presented in Table S2. Finally, the top 5 candidate peptides from both the R and XN-R sets were synthesized for experimental evaluation of their toxicity and efficacy in RANKL binding. The candidate peptides with good stability characteristics are shown in Figure S2 and the molecular structures of the candidate peptides are shown in Figure S3.

### ADMET-based toxicity evaluation of the candidate peptides

Toxicity represents a critical parameter in lead compound development. Given that computational prediction is a standard approach for preliminary toxicity assessment, we utilized ADMETlab 3.0 to evaluate the 10 candidate peptides identified from the above AI-driven screening. The predictions indicated that the majority of these peptides exhibit low or negligible toxicity. However, three candidate peptides, R-0037, XN-R3840, and XN-R3507, exhibit low hematotoxicity, and XN-R3855 has lower HEK293 cytotoxicity. It is noteworthy that XN-R4578 demonstrated extremely low toxicity across multiple assays, including hematotoxicity, RPMI-8226 immunotoxicity, and cytotoxicity in A549 and HEK293 cells, making it the top-performing candidate in the ADMET prediction (Table S3). None of the candidates were predicted to cross the blood-brain barrier. In addition to computational prediction, cytotoxicity was experimentally determined *in vitro* via the CCK-8 assay. Most candidate peptides, except R-1053, showed no significant cytotoxicity (Figure S4).

### Validation of R-Peptide and RANKL interaction

Following a comprehensive evaluation of the peptides' stability, molecular structure, ADMET properties, and cytotoxicity, their inhibitory effects on osteoclastogenesis were further assessed using TRAP staining (Figure S5). By integrating all the evaluations above, XN-R4578 was selected as the optimal candidate for further investigation. For convenience, it is designated as

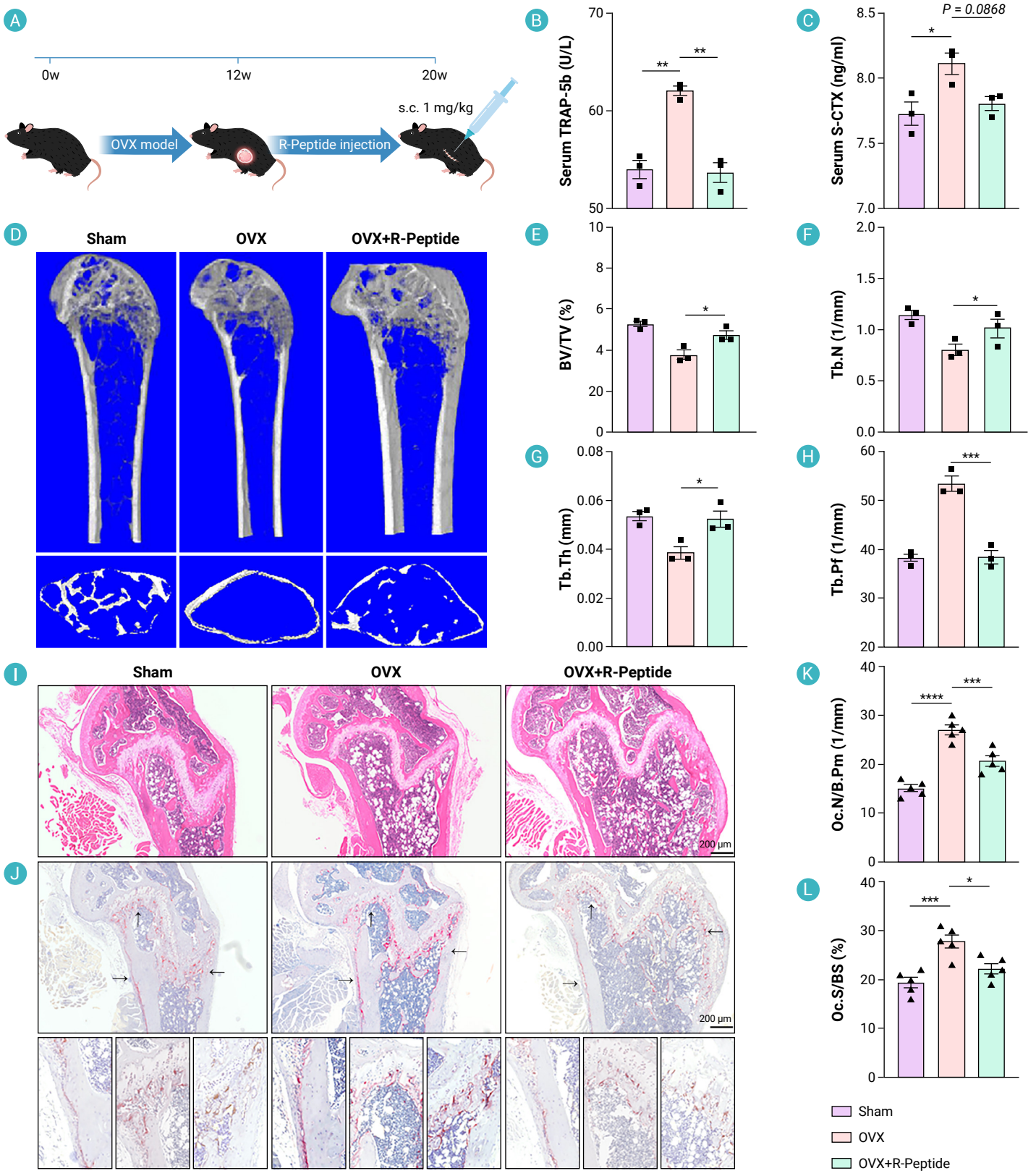



**Figure 4. Inhibition of bone resorption in OVX mice** (A) Schematic diagram of the OVX animal model and administration. Administer subcutaneously at a concentration of 1 mg/kg, five times per week for eight consecutive weeks. (B) Expression of TRAP-5b in serum, n = 3. (C) Expression of S-CTX in serum, n = 3. (D) Micro-CT results. (E) BV/TV quantitative chart, n = 3. (F) Tb.N quantitative chart, n = 3. (G) Tb.Th quantitative chart, n = 3. (H) Tb.Pf quantitative chart, n = 3. (I) HE staining results of bone sections. Scale bar, 200 μm. (J) TRAP staining results of bone section. Scale bar, 200 μm. The arrow indicates the area that is magnified locally. (K) Oc.N/B.Pm quantitative statistical chart, n = 5. (L) Oc.S/BS quantitative chart, n = 5. * $p < 0.05$, ** $p < 0.01$, *** $p < 0.001$, **** $p < 0.0001$

the R-Peptide in the following sections.

Next, we employed PyMOL to generate a schematic model of the candidate peptide docked into the RANKL binding site, visualizing its binding pose and identifying potential intermolecular contacts (Figure 2A). These amino acid residues, lysine 257, tyrosine 241, isoleucine 181, and histidine 180, represent potential binding sites for the R-peptide on RANKL. Notably, these

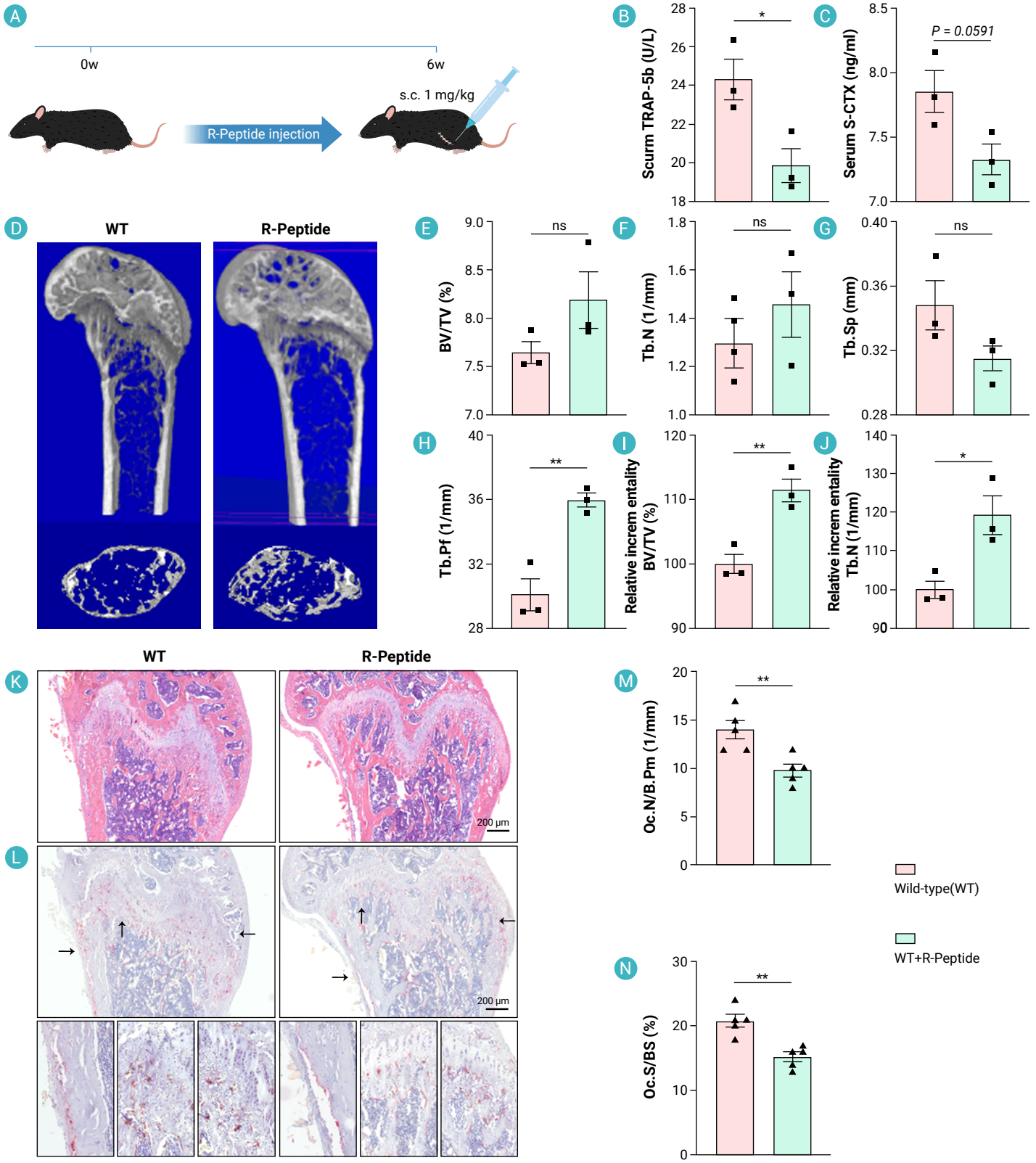



**Figure 5. Increase bone mass in WT mice** (A) Schematic diagram of WT animals and administration. Administer subcutaneously at a concentration of 1 mg/kg, five times per week for six consecutive weeks. (B) Expression of TRAP-5b in serum, n = 3. (C) Expression of S-CTX in serum, n = 3. (D) Micro-CT results. (E) BV/TV quantitative chart, n = 3. (F) Tb.N quantitative chart, n = 3. (G) Tb.Th quantitative chart, n = 3. (H) Tb.Pf quantitative chart, n = 3. (I) Quantitative statistical plot of the relative increment of BV/TV, n = 3. (J) Quantitative statistical plot of the relative increment of Tb.N, n = 3. (K) HE staining results of bone section. Scale bar, 200 μm. (L) TRAP staining results of bone section. Scale bar, 200 μm. The arrow indicates the area that is magnified locally. (M) Oc.N/B.Pm quantitative statistical chart, n = 5. (N) Oc.S/BS quantitative chart, n = 5. $^{ns}$ $p > 0.05$, $^{*}$ $p < 0.05$, $^{**}$ $p < 0.01$

sites differ from those targeted by small-molecule drugs [30], suggesting the possibility of developing novel therapeutics against RANKL through a distinct mechanism. To experimentally validate this interaction, we performed pull-down and co-immunoprecipitation (Co-IP) assays. For the pull-down assay, a biotinylated R-Peptide was synthesized. For the Co-IP assay, a His-tagged RP plasmid (designed based on the R-Peptide sequence) was constructed. In

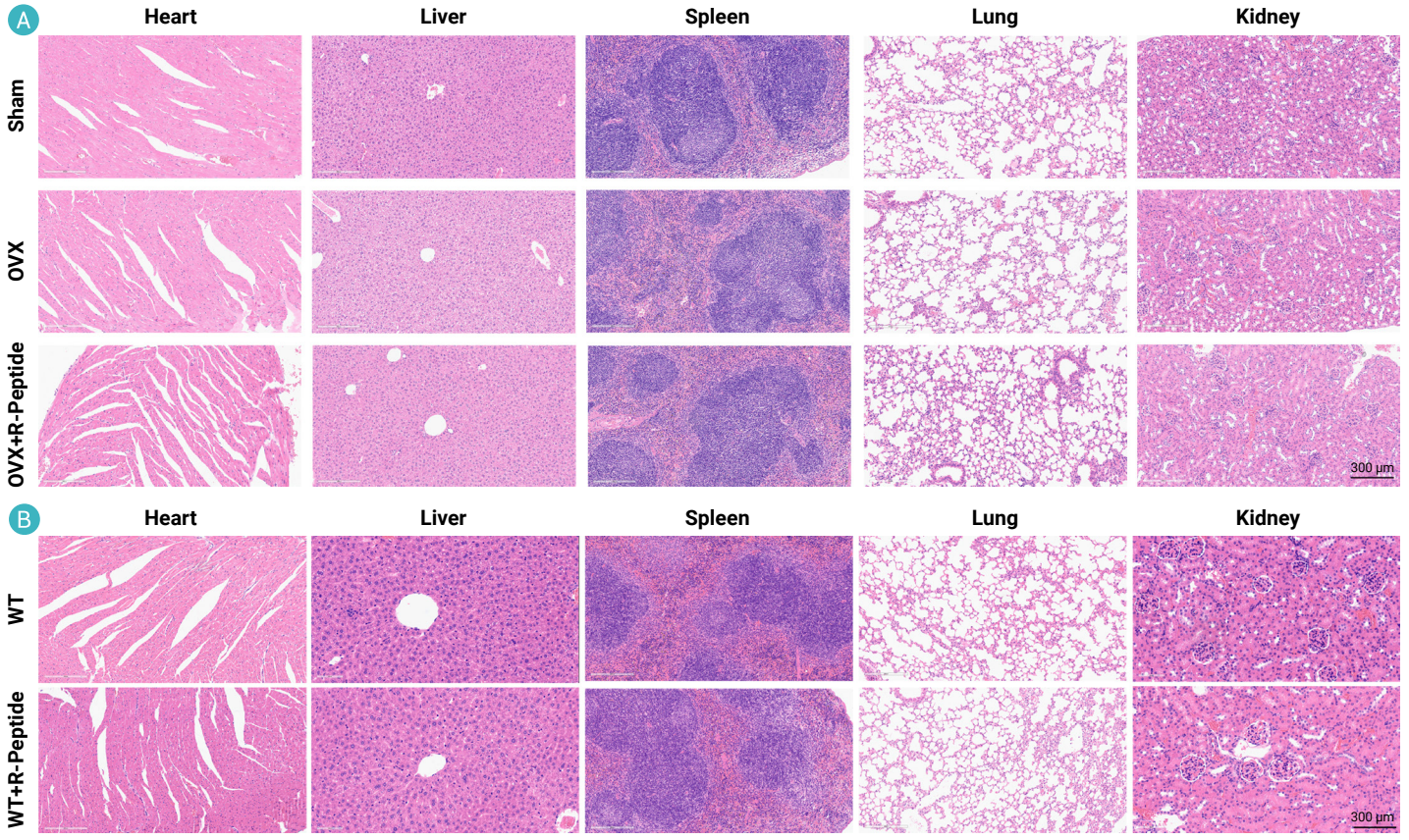



**Figure 6. HE staining results of heart, liver, spleen, lung and kidney tissue section of mice** (A) HE staining of various organs of OVX mice. (B) HE staining of various organs of Wide Type (WT) mice. Scale bar, 300 μm.

the pull-down assay, distinct biotin-positive bands appeared in the experimental lane (Lane 2) compared to the controls (Lane 1 and 3), representing the RANKL and R-Peptide complex and free biotinylated R-Peptide, respectively (Figure 2B). After profiling *Rankl* expression across multiple cell lines, MLOY-4 cells were chosen for intracellular binding assays due to their highest expression levels (Figure S6A). Therefore, cellular proteins were collected from MLOY-4 cells transfected with the His-RP plasmid (Fig.S6B) for Co-IP. Distinct bands in the experimental lane (Figure 2C, lane 2) were detected by anti-His tag antibody. Based on their molecular weights, the upper band denoted the RANKL and R-Peptide complex, while the lower band corresponded to the overexpressed R-Peptide. Subsequently, the same membrane was reprobed with anti-RANKL antibody. Bands were detected at positions corresponding to those seen in the anti-His blot (Figure 2D, lane 2). These Co-IP results confirmed that the R-Peptide interacts with RANKL. To further validate the effect of R-Peptide on RANKL-RANK interaction, we conducted His pull-down assays. His-tagged RANKL was first incubated with R-Peptide, followed by the addition of RANK. Subsequent analysis by Coomassie Brilliant Blue staining confirmed that the combined complex of R-Peptide and RANKL exists in the incubation product (Figure 2E). Subsequent Western blot analysis demonstrated that with the concentration increase of R-Peptide, more free RANK was released (Figure 2F). But the combined complex remained unchanged (Figure 2G). Collectively, these results demonstrate that R-Peptide inhibits RANKL function by disrupting the RANKL-RANK interaction.

## R-Peptide inhibits osteoclast differentiation

The activity and cytotoxicity of the R-Peptide were tested via the CCK-8 assay (Figure 3). The $IC_{50}$ value of the R-Peptide is approximately 1.7 μM (Figure 3A). The CCK-8 assay results showed no cytotoxicity between the cells in each group (Figure 3B). To examine the effect of R-Peptide on osteoclast differentiation, we performed TRAP staining (Figure 3C and Figure S5). We found that the numbers and the volume of osteoclasts were significantly reduced after the addition of the R-Peptide compared to the induction group (Figure 3D-E).

## R-Peptide inhibits bone resorption in OVX mice

The balance between osteoclasts and osteoblasts activity is crucial in bone remodeling, and its disruption can lead to bone diseases such as osteoporosis. The OVX animal model is a widely used tool in osteoporosis research. It induces abnormal bone metabolism by reducing systemic estrogen levels [1]. To evaluate the effect of the R-Peptide on bone resorption, we performed an *in vivo* study using OVX mice. The peptide was administered subcutaneously at a dose of 1 mg/kg, five times per week for eight consecutive weeks (Figure 4A). Serum TRAP-5b and S-CTX are established biomarkers of bone resorption. TRAP-5b is an enzyme secreted by osteoclasts and reflects osteoclast activity, whereas S-CTX is a degradation product of type I collagen that rises with increased bone resorption.[33-34] We therefore quantified their levels in mouse serum using ELISA. Compared with the OVX group, R-Peptide administration significantly reduced both serum TRAP-5b (Figure 4B) and S-CTX (Figure 4C) levels. Next, Micro-CT analysis was performed on the distal femur (Figure 4D). Overall, R-Peptide administration significantly improved bone microstructure compared to the OVX group, as evidenced by elevated BV/TV, Tb.N, and Tb.Th (Figure 4E-G) and a decrease in Tb.Pf (Figure 4H). To further evaluate the R-Peptide's effect, we performed HE staining and TRAP staining on femurs and quantified the TRAP-positive area (Figure 4I-J). Compared with the OVX group, R-Peptide administration significantly reduced both osteoclast number (Figure 4K) and osteoclast surface area (Figure 4L). Overall, these findings confirm that the R-Peptide effectively inhibits bone resorption *in vivo*.

## R-Peptide increases bone mass in WT mice

Currently, denosumab inhibits bone resorption by targeting RANKL, and studies have also found that denosumab may exert some inhibitory effects on bone formation.[35] To evaluate the effects of the R-Peptide on bone mass in mice, we performed a bone mass change test on WT mice (Figure 5A).

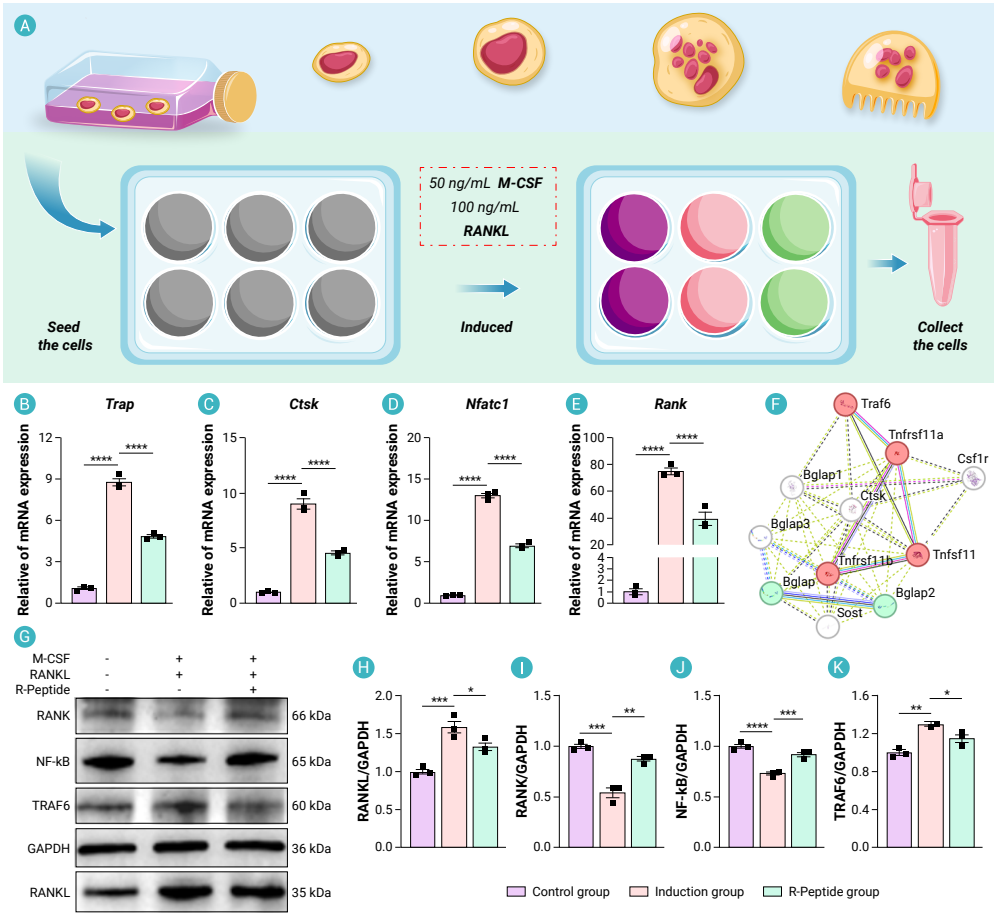



**Figure 7. Reduced osteoclast-related gene expression** (A) Schematic diagram of osteoclast induction. Relative gene expression analysis of (B) *Trap* and (C) *Ctsk* and (D) *Nfatc1* and (E) *Rank*. (F) Protein-protein interaction network diagram generated by STRING. (G) Western-blot result. Quantitative analysis of (H) RANKL and (I) RANK and (J) NF-κB and (K) TRAF6. * $p < 0.05$, ** $p < 0.01$, *** $p < 0.001$, **** $p < 0.0001$, n = 3.

Administer subcutaneously at a concentration of 1 mg/kg, five times per week for six consecutive weeks. First, we used an ELISA kit to detect the expression of TRAP-5b and S-CTX in mouse serum. Compared with the WT group, the expression of TRAP-5b was significantly decreased after the administration of the R-Peptide (Figure 5B), and the expression of S-CTX was also decreased (Figure 5C). Next, we performed a Micro-CT analysis of the lower limb femurs of mice (Figure 5D). Overall, the bone metabolic indexes were significantly changed after the administration of the R-Peptide. Compared with the WT group, we found that there was no statistically significant difference in the ratio of BV/TV and Tb.N after the administration of the R-Peptide, which may be due to the difference in the animals themselves (Figure 5E-F). The value of Tb.Sp was significantly decreased, and the value of Tb.Pf was significantly increased (Figure 5G-H). Therefore, we analysed the relative increments of the two groups, and we found that the relative increments of BV/TV and Tb.N showed significant differences, and both showed significant increases compared to the WT group (Figure 5I-J). To further evaluate the effect of the R-Peptide, we subsequently performed HE staining and TRAP staining on the femur, and quantified the TRAP staining results (Figure 5K-L). We can see that the number of osteoclasts (Figure 5M) and osteoclast surface (Figure 5N) decreased significantly after the administration of the R-Peptide compared to the control mice. Overall, wild-type (WT) mice exhibited increased bone mass following injection of the R-Peptide.

## The safety evaluation of the R-Peptide in vivo

To assess the animal safety of the R-Peptide. We collected pathological sections from the heart, liver, spleen, lung, and kidney tissue section of OVX and WT mice and then performed HE staining. We found that, compared with the model group, there was no damage to these organs after administration of the R-Peptide (Figure 6A-B). To further evaluate whether R-Peptide inhibits the immune response in mice, we performed immunofluorescence (IF) staining on spleen sections from OVX mice (Figure S7A). CD4 and CD8, two key marker molecules on the surface of T lymphocytes, play a crucial role in the immune system, and their ratio (CD4/CD8) serves as a key indicator for assessing immune status. Compared to OVX mice, mice treated with R-Peptide exhibited a significant increase in the area of CD4+ cell expression in the spleen (Figure S7B). Consistently, the CD4+/CD8+ ratio showed an upward trend (Figure S7C). These findings indicate that R-Peptide administration did not induce immunosuppression in mice. Conversely, it enhanced CD4+ expression in the experimental group (OVX + R-Peptide). Furthermore, we examined the levels of TNF-α and IL-6, well-established inflammatory mediators, in bone, spleen, liver, and kidney tissue sections from OVX mice. There was no significant change in the fluorescence intensity of TNF-α and IL-6 following R-Peptide administration compared to the OVX group (Figure S8). The above results demonstrate that R-Peptide administration activates, rather than suppresses, the immune system.

## R-Peptide reduces the expression of osteoclast-related genes

To investigate the *in vitro* mechanism of action of the R-Peptide, we performed an osteoclast induction assay using primary mouse bone marrow mesenchymal stem cells (Figure 7A). Total RNA was collected from the cells, and the expression of osteoclast-related genes *Trap*, *Ctsk*, *Nfatc1* and *Rank* was detected by qPCR assay (Figure 7B-E). We found that the expression of *Trap*, *Ctsk*, *Nfatc1* and *Rank* genes was significantly decreased after the addition of the R-Peptide compared with the induction group. The OPG-RANKL-RANK and TRAF6-RANKL-NF-kB signaling pathways are currently two important signaling pathways widely involved with RANKL. The OPG-RANKL-RANK signaling pathway mediates the bone remodeling process,[36] while the TRAF6-RANKL-NF-kB signaling pathway mediates osteoclast differentiation.[37] RANK is the receptor activator of NF-kB and also serves as the receptor for osteoclast activation, playing an important role in osteoclast differentiation. So, we used STRING software to display the interaction network among the above proteins. The results are shown in Figure 7F. To further verify the effect of the R-Peptide. We collected the proteins and analyzed their expression levels via Western-blot assay (Figure 7G). Compared with the induction group, we found that the protein expression of RANKL and TRAF6 was significantly reduced after adding the R-Peptide (Figure 7H-K). The protein expression of RANK and NF-κB was significantly increased (Figure 7I-J), and the protein expression results were consistent with the gene expression results. Therefore, we speculate that the R-Peptide inhibits osteoclast function by affecting RANK-RANKL interactions through acting on RANKL, thereby inhibiting the function of osteoclasts.

## DISCUSSION

Bone resorption is essential for maintaining skeletal development, but excessive resorption leads to abnormal development of the bone's internal structure. One of the main reasons for the occurrence of osteoporosis lies in the overwhelming dominance of osteoclast-mediated bone resorption, breaking the relative homeostatic balance between bone resorption and bone formation. As a degenerative disease, it poses a serious threat to the quality of life of the elderly [3]. Drug development targeting disease-related targets and cells represents a novel strategy in the field of new drug discovery,[38]

which has been applied in basic research. Currently, developing agonist or antagonist drugs for disease treatment based on the target structure has become a hot research topic.

Peptide drugs for treating osteoporosis, such as teriparatide[17] and abaloparatide,[18] promote bone formation by acting on the parathyroid hormone receptor (PTHR). Research has revealed a significant limitation of teriparatide: its therapeutic window.[4,39] Based on this, developing novel peptide drugs to slow bone resorption or promote bone formation will help improve the quality of life for osteoporosis patients. At present, peptide library screening and virtual docking strategies have been applied to the development of drugs. With the development of artificial intelligence (AI) algorithms and the emergence of various large language models, AI algorithm models are playing an increasingly critical role in the process of assisting drug discovery.[25,27-28] Compared to traditional drug development, AI+ technology significantly accelerates the drug discovery process.[16,26]

This study employed a virtual docking strategy, utilizing artificial intelligence algorithm models to screen peptide sequences exhibiting high affinity for the RANKL targets.[40] Then, a large language model was applied to perform machine learning on the peptide sequences with the favorable docking results, thereby constructing a novel virtual peptide library.[38] By establishing a candidate peptide library, novel peptides with bone resorption inhibitory effects were identified, and their potential for treating osteoporosis was further explored. In this study, the candidate peptides were preliminarily validated through *in vitro* experiments, revealing their ability to inhibit osteoclast differentiation. Subsequently, the R-Peptide underwent *in vivo* evaluation using OVX mice. Furthermore, by validating the classical signaling pathway TRAF6-RANKL-NF-κB, we propose at the cellular level that this peptide may exert its effects by interacting with RANKL, thereby influencing RANKL-RANK interactions. This subsequently alters bone resorption capacity, ultimately inhibiting osteoclast differentiation. Finally, we evaluated the peptide's effect on bone formation capacity in wild-type mice, with particular focus on its impact on bone mass.

However, there are several limitations in this study, such as: the insufficient number of peptides in the peptide library, the lack of in-depth investigation into the specific mechanism of action, etc. In general, we successfully discovered and identified a peptide that has the ability to inhibit osteoclast resorption, and validated the efficacy of the R-Peptide in both *in vitro* and *in vivo* experiments, providing a novel therapeutic strategy for osteoporosis.

## Declaration of generative AI in the writing process

During the writing process, we used an online AI tool—DeepSeek (https://chat.deepseek.com) and DeepL (https://www.deepl.com) to improve readability and language. And then we carefully reviewed and edited the manuscript.

## REFERENCES


1. Salhotra, A., Shah, H. N., Levi, B., et al. (2020). Mechanisms of bone development and repair. *Nat. Rev. Mol. Cell. Biol.* **21**:696–711. DOI:10.1038/s41580-020-00279-w
2. Lv, X., Gao, F., and Cao, X. (2022). Skeletal interoception in bone homeostasis and pain. *Cell. Metab.* **34**:1914–1931. DOI:10.1016/j.cmet.2022.09.025
3. Xiang, Q., Li, L., Ji, W., et al. (2024). Beyond resorption: osteoclasts as drivers of bone formation. *Cell. Regen.* **13**:22. DOI:10.1186/s13619-024-00205-x
4. Foessl, I., Dimai, H. P., and Obermayer-Pietsch, B. (2023). Long-term and sequential treatment for osteoporosis. *Nat. Rev. Endocrinol.* **19**:520–533. DOI:10.1038/s41574-023-00866-9
5. Walker, M. D., and Shane, E. (2023). Postmenopausal Osteoporosis. *N. Engl. J. Med.* **389**:1979–1991. DOI:10.1056/NEJMcp2307353
6. Reid I. R. (2020). A broader strategy for osteoporosis interventions. *Nat. Rev. Endocrinol.* **16**:333–339. DOI:10.1038/s41574-020-0339-7
7. Tsai, J., Kaneko, K., Suh, A. J., et al. (2023). Origin of Osteoclasts: Osteoclast Precursor Cells. *J. Bone. Metab.* **30**:127–140. DOI:10.11005/jbm.2023.30.2.127
8. Elson, A., Anuj, A., Barnea-Zohar, M., et al. (2022). The origins and formation of bone-resorbing osteoclasts. *Bone.* **164**:116538. DOI:10.1016/j.bone.2022.116538
9. Ono, T., Hayashi, M., Sasaki, F., et al. (2020). RANKL biology: bone metabolism, the immune system, and beyond. *Inflamm Regen.* **40**:2. DOI:10.1186/s41232-019-0111-3
10. Ikebuchi, Y., Aoki, S., Honma, M., et al. (2018). Coupling of bone resorption and formation by RANKL reverse signalling. *Nature.* **561**:195–200. DOI:10.1038/s41586-018-0482-7
11. Cao X. (2018). RANKL-RANK signaling regulates osteoblast differentiation and bone formation. *Bone. Res.* **6**:35. DOI:10.1038/s41413-018-0040-9
12. Bae, S., Kim, K., Kang, K., et al. (2023). RANKL-responsive epigenetic mechanism reprograms macrophages into bone-resorbing osteoclasts. *Cell. Mol. Immunol.* **20**:94–109. DOI:10.1038/s41423-022-00959-x
13. Wu, Q., Qian, W., Sun, X., et al. (2022). Small-molecule inhibitors, immune checkpoint inhibitors, and more: FDA-approved novel therapeutic drugs for solid tumours tumors from 1991 to 2021. *J. Hematol. Oncol.* **15**:143. DOI:10.1186/s13045-022-01362-9
14. Sun, X., Setrerrahmane, S., Li, C., et al. (2024). Nucleic acid drugs: recent progress and future perspectives. *Signal. Transduct. Target. Ther.* **9**:316. DOI:10.1038/s41392-024-02035-4
15. Carter, P. J., and Rajpal, A. (2022). Designing antibodies as therapeutics. *Cell.* **185**:2789–2805. DOI:10.1016/j.cell.2022.05.029
16. Muttenthaler, M., King, G. F., Adams, D. J., et al. (2021). Trends in peptide drug discovery. *Nat. Rev. Drug. Discov.* **20**:309–325. DOI:10.1038/s41573-020-00135-8
17. Kendler, D.L., Marin, F., Zerbini, C.A.F., et al. (2018). Effects of teriparatide and risedronate on new fractures in post-menopausal women with severe osteoporosis (VERO): a multicentre, double-blind, double-dummy, randomised controlled trial. *Lancet.* **391**:230–240. DOI:10.1016/S0140-6736(17)32137-2
18. Miller, P.D., Hattersley, G., Riis, B.J., et al. (2016). Effect of Abaloparatide vs Placebo on New Vertebral Fractures in Postmenopausal Women With Osteoporosis: A Randomized Clinical Trial. *JAMA.* **316**:722–733. DOI:10.1001/jama.2016.11136
19. Shukla, A. K., and Bhavya, B. (2025). Tirzepatide for Obesity Treatment and Diabetes Prevention. *N. Engl. J.Med.* **392**:2492. DOI:10.1056/NEJMc2504728
20. Apostolopoulos ,V., Bojarska, J., Chai, T.T.,et al. (2021). A Global Review on Short Peptides: Frontiers and Perspectives. *Molecules.* **26**:430. DOI:10.3390/molecules26020430
21. Jakubczyk, A., Karaś, M., Rybczyńska-Tkaczyk, K., et al. (2020). Current Trends of Bioactive Peptides-New Sources and Therapeutic Effect. *Foods.* **9**:846. DOI:10.3390/foods9070846
22. Atanasov, A. G., Zotchev, S. B., Dirsch, V. M., et al. (2021). Natural products in drug discovery: advances and opportunities. *Nat. Rev. Drug. Discov.* **20**:200–216. DOI:10.1038/s41573-020-00114-z
23. Ancajas, C. M. F., Oyedele, A. S., Butt, C. M., et al. (2024). Advances, opportunities, and challenges in methods for interrogating the structure activity relationships of natural products. *Nat. Prod. Rep.* **41**:1543–1578. DOI:10.1039/d4np00009a
24. Rudrapal M, and Chetia D. (2020). Virtual Screening, Molecular Docking and QSAR Studies in Drug Discovery and Development Programme. *J. Drug. Deliv. Sci. Tec.* **10**:225–233. DOI:10.22270/jddt.v10i4.4218
25. Shen, J., Jiang, J., Kuang, G., et al. (2012). Discovery and structure-activity analysis of selective estrogen receptor modulators via similarity-based virtual screening. *Eur. J. Med. Chem.* **54**:188–196. DOI:10.1016/j.ejmech.2012.04.041
26. Gorgulla, C., Boeszoermenyi, A., Wang, Z.F., et al. (2020). An open-source drug discovery platform enables ultra-large virtual screens. *Nature.* **580**:663–668. DOI:10.1038/s41586-020-2117-z
27. Xue, B., Li, R., Cheng, Z., et al. (2024). High-Affinity Peptides for Target Protein Screened in Ultralarge Virtual Libraries. *ACS. Cent. Sci.* **10**:2111–2118. DOI:10.1021/acscentsci.4c01385
28. Adeshina, Y. O., Deeds, E. J., and Karanicolas, J. (2020). Machine learning classification can reduce false positives in structure-based virtual screening. *Proc. Natl. Acad. Sci. U. S. A.* **117**:18477–18488. DOI:10.1073/pnas.2000585117
29. Forli, S., Huey, R., Pique, M. E., et al. (2016). Computational protein-ligand docking and virtual drug screening with the AutoDock suite. *Nat. Protoc.* **11**:905–919. DOI:10.1038/nprot.2016.051
30. Huang, D., Zhao, C., Li, R., et al. (2022). Identification of a binding site on soluble RANKL that can be targeted to inhibit soluble RANK-RANKL interactions and treat osteoporosis. *Nat. Commun.* **13**:5338. DOI:10.1038/s41467-022-33006-4
31. Liang, W., Feng, R., Li, X., et al. (2024). A RANKL-UCHL1-sCD13 negative feedback loop limits osteoclastogenesis in subchondral bone to prevent osteoarthritis progression. *Nat. Commun.* **15**:8792. DOI:10.1038/s41467-024-53119-2
32. Trajanoska, K., Bhérer, C., Taliun, D., et al. (2023). From target discovery to clinical drug development with human genetics. *Nature.* **620**:737–745. DOI:10.1038/s41586-023-06388-8
33. Terreni, A., and Pezzati, P. (2012). Biochemical markers in the follow-up of the osteoporotic patients. *Clin. Cases. Miner. Bone. Metab.* **9**:80–84. ..
34. Vasikaran, S., Eastell, R., Bruyère, O., et al. (2011). Markers of bone turnover for the prediction of fracture risk and monitoring of osteoporosis treatment: a need for international reference standards. *Osteoporos. Int.* **22**:391–420. DOI:10.1007/s00198-010-1501-1
35. Ishikawa, K., Tani, S., Sakai, N., et al. (2025). Mouse model of anti-RANKL discontinuation reveals reduced bone mass and quality through disruption of bone remodelling remodeling. *Bone. Res.* **13**:56. DOI:10.1038/s41413-025-00433-0
36. Boyce, B. F., and Xing, L. (2008). Functions of RANKL/RANK/OPG in bone modeling and remodeling. *Arch. Biochem. Biophys.* **473**:139–146. DOI:10.1016/j.abb.2008.03.018
37. Anzai, M., Watanabe-Takahashi, M., Kawabata, H., et al. (2025). Clustered peptide regulating the multivalent interaction between RANK and TRAF6 inhibits osteoclastogenesis by fine-tuning signals. *Commun. Biol.* **8**:643. DOI:10.1038/s42003-025-08047-2

38. Miller, P. D., Lewiecki, E. M., Krohn, K., et al. (2021). Teriparatide: Label changes and identifying patients for long-term use. *Cleve. Clin. J. Med.* **88**:489–493. DOI:10.3949/ccjm.88a.21011
39. Goles, M., Daza, A., Cabas-Mora, G., et al. (2024). Peptide-based drug discovery through artificial intelligence: towards an autonomous design of therapeutic peptides. *Brief. Bioinform.* **25**:bbae275. DOI:10.1093/bib/bbae275
40. Cai, M., Xiao, B., Jin, F., et al. (2022). Generation of functional oligopeptides that promote osteogenesis based on unsupervised deep learning of protein IDRs. *Bone. Res.* **10**:23. DOI:10.1038/s41413-022-00193-1

## FUNDING AND ACKNOWLEDGMENTS

We thank Lei Hu and Huan Liu for their insightful discussions and constructive suggestions throughout this work. This work was supported by the National Natural Science Foundation of China (No. 82350003 and 82072499).

## AUTHOR CONTRIBUTIONS

Z.C.: Methodology, Investigation, Formal analysis, Interpretation, Visualization, Validation, Writing - original draft, and Writing - review and editing. Z.L.: Methodology and Data collection. Y.C.: Investigation, Data collection, Formal analysis, and Interpretation. Y.Y. and C.W.: Data collection and Formal analysis. C.L. and X.W.: Conceptualization, Supervision, Project management, Funding acquisition, Interpretation, and Writing - review and editing. All authors have reviewed the final manuscript and approved its submission.

## DECLARATION OF INTERESTS

Xiaogang Wang is an Editorial Board member of The Innovation Drug Discovery and was blinded from reviewing or making final decisions on the manuscript. Peer review was handled independently of this member and their research group. The other authors declare no conflicts of interest.

## ETHICAL STATEMENT AND PATIENT CONSENT

All animal experiments were conducted in accordance with the ARRIVE guidelines for reporting animal experiments. Euthanasia was performed by cervical dislocation under deep anesthesia. All experimental procedures were approved by the Biological and Medical Ethics Committee of Beihang University (Approval No. BM20210142).

## DATA AND CODE AVAILABILITY

The data that support the findings of this study are available from the corresponding author upon reasonable request.

## SUPPLEMENTAL INFORMATION

It can be found online at https://doi.org/10.59717/j.xinn-drugdisc.2026.100041.